

# Enhanced thermoelectric properties in phosphorene nanorings

Fatemeh Moghadasi Borojeni<sup>1</sup>, Esmaeil Taghizadeh Sisakht<sup>1</sup>, Farhad Fazileh<sup>1,\*</sup> and F. M. Peeters<sup>2,3</sup>

<sup>1</sup>*Department of Physics, Isfahan University of Technology, Isfahan 84156-83111, Iran*

<sup>2</sup>*HSE University, Moscow, 10100 Russia and*

<sup>3</sup>*Departamento de Física, Universidade Federal do Ceara, 60455-760 Fortaleza, Ceara, Brazil*

(Dated: December 21, 2022)

Using the tight-binding approach, we investigate the thermoelectric properties of rectangular phosphorene nanorings for both symmetrically and asymmetrically attaching to phosphorene nanoribbon leads. We design our phosphorene-based nanostructures to enhance the thermoelectric performance in the absence and the presence of perpendicular magnetic fields. Our results show that when zigzag phosphorene nanoribbons (ZPNRs) are coupled symmetrically to rectangular rings, a comparatively large band gap is induced in the electronic conductance due to the suppression of the contribution of edge states. This gives rise to a remarkable increase in the thermopower response compared to the case of pristine ZPNRs. More intriguingly, we found that though the maximum power factor in this system is about the same as the one for its ZPNR counterpart, the much smaller electronic thermal conductance of this phosphorene-based nanostructure can remarkably contribute to the improvement of the figure of merit. Also, we found that the symmetry/asymmetry of our designed nanostructures, the geometrical characteristics of the ring, and the magnetic flux are three important factors that control the thermoelectric properties of phosphorene quantum rings. Our numerical calculations show that by changing the magnetic flux through the nanoring, a drastic increase in the thermopower is observed near an antiresonance point. We demonstrate the tunability of the thermopower and the possibility to switch on and off the thermoelectric response of phosphorene nanorings with the magnetic flux. Moreover, for asymmetric connection configurations with armchair-edged leads, we found that though the thermopower is almost intact, a remarkable reduction of the electronic thermal conductance can lead to a notable improvement in the figure of merit. Our results suggest phosphorene nanorings as promising candidate nanostructures for thermoelectric applications.

## I. INTRODUCTION

Designing devices with optimal thermoelectric (TE) properties is highly desirable for the future of energy harvesting and environmental issues [1]. TE materials occupy a special place in clean energy research field, since they directly convert heat into electrical energy and vice versa. They are promising candidate materials for the future of clean and efficient electrical power generators and cooling (heating) devices. The TE efficiency of a material is often assessed by dimensionless figure of merit  $ZT = \frac{S^2 \sigma T}{\kappa}$ ; where  $S$  is the Seebeck coefficient (SC) or thermopower,  $\sigma$  and  $\kappa$  are the electrical and thermal conductivities, respectively and  $T$  is the temperature. This relation suggests that a reduction in thermal conductivity (while the electrical conductivity is kept almost the same) leads to a strong improvement of the TE efficiency. One way to accomplish this task is to make nanostructures out of the bulk TE materials [2]. Here, the enhanced TE factor of merit  $ZT$  is due to phonon scattering with boundaries and quantum confinement effects. The TE efficiency can be further enhanced by making nanorings out of the materials [3, 4]. Using nanorings made of nanoribbons of the pristine materials we can take advantage of the Aharonov-Bohm (AB) effect when we apply an external magnetic field to tune the magnetoresistance of the system [5] and further enhance the TE efficiency [6, 7].

Among nanostructured semiconducting materials, two dimensional (2D) phosphorene has recently received remarkable attention due to its great transport properties and potential applications [8–15]. This structure consists of a single- or few-layer of black phosphorus and has been successfully fabricated by researchers [10, 11, 14]. From these studies, it is suggested that because of its remarkable electronic, mechanical, and optical properties, it offers great promise for applications in electronic and optoelectronic devices [16–25]. In addition, due to superior thermoelectric characteristics, it is also proposed that phosphorene nanostructures are highly promised for thermoelectric devices and it could be their key application in the future [26]. Various factors may significantly affect the three parameters that are used to quantify the figure of merit in this structure. For single-crystals of bulk black phosphorus, the experimental measurements revealed that the value of SC is about  $340 \mu\text{V}/\text{K}$  at room temperature [27]. It was shown that gate-tuning is a successful way to control the TE power coefficient in a thin flake of black phosphorus [28]. These experimental measurements verified that the SC of the ion-gated bulk black phosphorus can reach  $510 \mu\text{V}/\text{K}$  at 210 K which may result in a great increase of  $ZT$  compared to the bulk single crystal at room temperature. The puckered structure of monolayer phosphorene has led to anisotropy in its electrical and thermal properties [29]. Theoretical studies showed that this distinct feature gives rise to orthogonal electrical and thermal conductances [30]. This results in a higher  $\sigma/\kappa$  ratio and thus the rather large

\* fazileh@iut.ac.ir

figure of merit  $ZT \sim 1$  (at room temperature) along the armchair direction of monolayer phosphorene [30]. Moreover, it is traditionally believed that the utilization of the nanoribbons of such 2D materials is a way to enhance the TE efficiency. Theoretical calculations predicted that using phosphorene nanoribbons (PNRs) as thermoelectric material can lead to improved TE efficiencies [31]. In addition, the effect of the edge states on the thermopower in zigzag phosphorene nanoribbons (ZPNRs) was studied [32]. It was shown that by applying a transverse electric field, one can completely push the edge modes into the bulk bands and maximize the bulk energy gap which results in enhanced thermoelectric power in PNRs [32]. Also, it was found that the passivation of edge phosphorous atoms with hydrogen in both types of nanoribbon edges [31], and even oxidation in phosphorene oxide [33] enhances the thermopower.

These studies confirm that nanoribbon-based structures of monolayer phosphorene are likely candidates to improve the TE properties and the advent of efficient TE nanodevices. Recent studies reported the production of high-quality PNRs with relatively large and uniform lengths that may renew the interest in the study of thermoelectric properties in nanoribbons and nanostructured systems made of phosphorene [34]. Nanorings made of two dimensional materials are possible nanostructures that may be used to improve TE efficiency. For example, TE properties of rectangular graphene nanorings have been investigated for different conditions and are proposed to build tunable TE generators [3, 35]. In such systems, the improvement in the TE performance is attributed to the emergence of Fano line shapes or Breit-Wigner line shapes in the transmission coefficient that their behavior depends on the geometrical characteristics of the ring and the applied side-gate voltage [3]. However, despite the numerous works [28–33] on the TE properties of phosphorene and phosphorene nanoribbons, the TE performance of rectangular phosphorene nanorings has remained elusive so far.

In the present work, inspired by the mentioned methods to improve the TE performance in graphene nanorings, we investigate the thermoelectric characteristics of rectangular phosphorene nanorings for both symmetrically and asymmetrically attachment to the leads. We investigate the effect of an applied external magnetic field on the TE properties of these rectangular rings and show how the thermoelectric coefficients are controllable in our designed systems by the magnetic field. Also, we examine the role of ring size and the symmetry of the connection configuration of leads on the TE response of these systems. Our results will reveal the desirability of these phosphorene-based nanostructures in designing efficient TE devices.

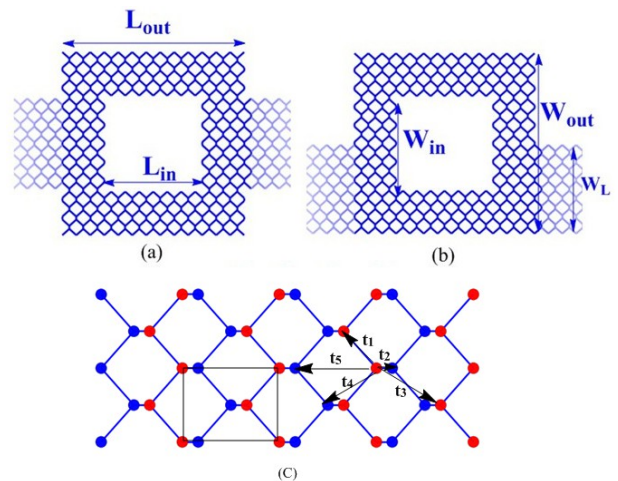


FIG. 1. (a) and (b) show the schematic of symmetric and asymmetric coupling of a rectangular phosphorene ring to two leads. The geometrical parameters of the system are shown (c) Lattice structure of monolayer phosphorene (top view). There are four P atoms in the rectangular primitive unit cell of monolayer phosphorene. Red and blue balls denote the puckered structure of the system.  $t_1$ - $t_5$  denote the used hopping parameters in our TB model.

## II. MODEL AND FORMALISM

The system under study is a rectangular phosphorene nanoring with a symmetric or asymmetric coupling to two leads as shown in Figs. 1(a) and (b). In each configuration, two semi-infinite zigzag- or armchair-edged nanoribbon of phosphorene connect to a nanoring. The geometry of a rectangular quantum ring is determined by the inner and outer sides  $L_{in}$ ,  $W_{in}$ ,  $L_{out}$ , and  $W_{out}$ . Ma et al. [32] showed that by adjusting the bias voltage of a zigzag phosphorene nanoribbon, the midgap bands completely split and the corresponding localized states give rise to an enhancement in the thermopower. We connect two ZPNRs to the phosphorene nanoring to show that a wide band gap can be induced. This is accompanied by a drastic increase in the magnitude of thermopower compared with the case without the nanoring and even compared with graphene nanorings. In monolayer phosphorene (MLP), each phosphorus atom (P) is covalently bonded to three neighbor phosphorus atoms and form a puckered structure as depicted in Fig. 1 (c). The lattice constants of MLP are  $a = 4.38\text{\AA}$ , and  $b = 3.31\text{\AA}$ . There are four P atoms in the rectangular primitive unit cell of MLP. The generally accepted low-energy tight-binding (TB) Hamiltonian for MLP is given by [36]

$$H_c = \sum_{i \neq j} t_{ij} c_i^\dagger c_j, \quad (1)$$

which can also be used to construct the Hamiltonian of PNRs with bare edges. By applying a perpendicular magnetic field  $B$  to the plane of a MLP nanoring, the

hopping parameters  $t_{ij}$  in Eq. (1) are substituted by

$$t_{ij} \rightarrow t_{ij} \exp\left(i \frac{2\pi e}{h} \int_{\mathbf{r}_i}^{\mathbf{r}_j} \mathbf{A} \cdot d\mathbf{l}\right), \quad (2)$$

to include Peierl's phase factor, where  $\mathbf{A}$  is the vector potential. To calculate the quantum conductance of a MLP nanoring, we utilize the Landauer-Buttiker formalism as implemented in the KWANT [37] package. In this approach, the ballistic transport of charge carriers through a nanoring is given by

$$G = \frac{2e^2}{h} \int \left(-\frac{\partial f_0}{\partial E}\right) T_{LR}(E) dE. \quad (3)$$

In this equation,  $f_0$  is the Fermi distribution function  $1/[e^{(E-E_f)/k_B T} + 1]$  at temperature  $T$ , and  $T_{LR}(E)$  denotes the transmission coefficient of our lead-nanoring-lead system [38, 39]. The thermopower  $S$  and the electronic contribution to thermal conductance  $\kappa_e$  are expressed in terms of the moments of the transmission coefficient [40]

$$K_n = \frac{2}{h} \int_{-\infty}^{\infty} \left(-\frac{\partial f_0}{\partial E}\right) (E - \mu)^n T_{LR}(E) dE, \quad (4)$$

via the following equations

$$S = -\frac{1}{eT} \frac{K_1}{K_0}, \quad (5)$$

$$\kappa_e = \frac{1}{T} \left[ K_2 - \frac{K_1^2}{K_0} \right]. \quad (6)$$

To construct the TB models in our systems, we employed the Pybinding code package [41].

### III. RESULTS

We design our phosphorene-based nanostructures to enhance the TE performances compared to the TE responses of pristine PNRs. So, before proceeding with our main systems, we first examine the electronic conductance  $G$ , the Seebeck coefficient  $S$ , the electronic thermal conductance  $\kappa_e$ , and the thermoelectric power factor  $PF=G S^2$  for pristine PNRs. Figures 2(a1)-(a2) and 2(b1)-(b2) show the calculated conductance and thermopower for a typical armchair phosphorene nanoribbon (APNR) and ZPNR, respectively. We set the width of ribbons to  $W = 8$  nm for both APNRs and ZPNRs. The intriguing electronic properties of APNRs and ZPNRs have a direct consequence on their transport characteristics. As shown in Figs. 2(a1) and (b1), the conductance of both APNRs and ZPNRs exhibit quantized plateaus  $G = ne^2/h$ , where  $e^2/h$  is the conductance quantum and  $n$  denotes the number of available transport modes at energy  $E$ . As seen, the ZPNR shows a conductance plateau

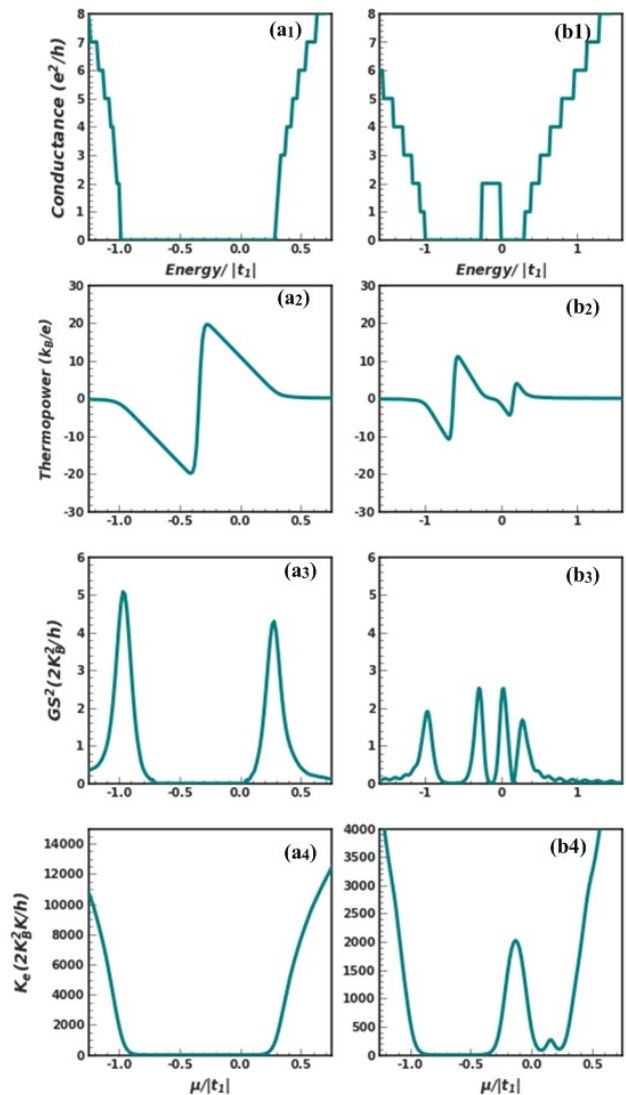


FIG. 2. (a1)-(a4) electronic conductance, thermopower, electronic thermal conductance, and power factor a function of chemical potential for a APNR with  $W = 8$  nm. The temperature is set to  $k_B T = 0.03|t_1|$  in our calculations. (b1)-(b4) the same quantities for a ZPNR with  $W = 8$  nm and at  $k_B T = 0.03|t_1|$ .

of value  $G = 2e^2/h$  near the zero energy region because of the contribution of edge-propagating states along the zigzag boundaries. On the other hand, due to the absence of propagating edge modes in the APNR, there exists no quantized plateau in the midgap region. Furthermore, the lack of electron-hole symmetry in the electronic band structures of PNRs leads to an asymmetry of their quantum conductance with respect to  $E = 0$ . Figures 2(a2) and (b2) depict the numerically calculated thermopower  $S$ . A comparison between the thermopower of the APNR and ZPNR shows that the presence of mid-gap edge modes drastically affects the SC, and hence it is sensitive to the topology of the boundaries in a PNR. We have shown in Figs. 2(a3) and (b3) the peaks of the

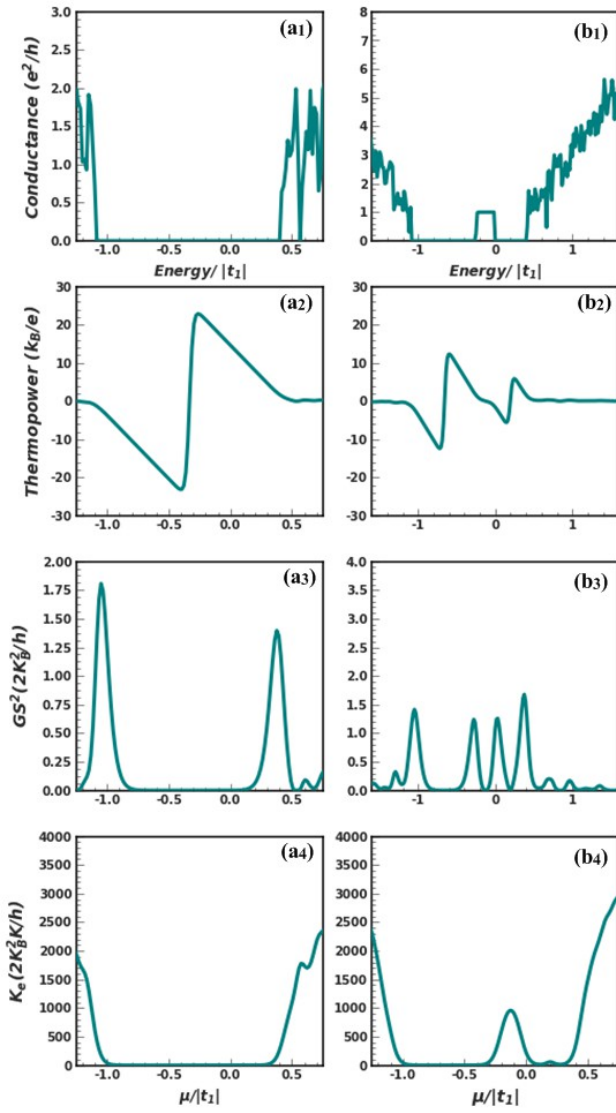


FIG. 3. (a1)-(a4) electronic conductance, thermopower, electronic thermal conductance, and power factor a function of chemical potential for a symmetric PRZL. The parameters are set to  $k_B T = 0.03|t_1|$ ,  $B = 0$ ,  $W_{in} = L_{in} = W_{out}/2 = L_{out}/2 = W_L = 8$  nm. (b1)-(b4) the same quantities for an asymmetric PRZL with the same set of parameters.

power factor for the condition in which chemical potential sets close to the transmission gap. Also, Figs. 2(a4) and (b4) display the electronic thermal conductance  $\kappa_e$  as a function of the chemical potential  $\mu$ . As seen, due to the lack of electron-hole symmetry,  $\kappa_e$  is also asymmetric around  $\mu = 0$ . To enhance the SC in phosphorene, one way is to induce a large band gap in phosphorene nanostructures with zigzag edges that have metallic characteristic. This can be achieved by connecting two narrow leads of PNR to a rectangular phosphorene nanoring as schematically depicted in Fig. 1. We couple two PNRs with zigzag edges to a rectangular ring to present the mentioned quantities for both symmetric (Figs. 3(a1)-

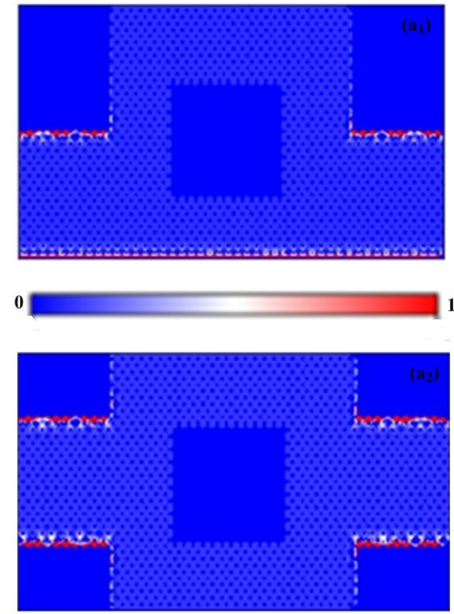


FIG. 4. Spatial LDOS for (a) a symmetric and (b) an asymmetric PRZL at  $E_f = 0$  eV. The color bar denotes the electronic density distributions across the device.

(a4)) and asymmetric (Figs. 3(b1)-(b4)) configurations. It is found that for a symmetric connection configuration, the conductance and thermopower are considerably affected compared to the case of pristine PNRs. A comparison between the SCs in Figs. 3(a2) and 2(b2) shows that in this case, the absolute value of the maxima is notably greater than that of the ZPNR counterpart. By comparing Figs. 2(b1) and 3(a1), one can see that for the symmetric case, the first conductance plateau in ZPNR disappears completely, which is understood as an induced large band gap in the electronic conductance due to the suppression of the contribution of edge states. We have shown in Fig. 4(a1) the electronic local density of states (LDOS) for a symmetric PRZL at  $E = 0$  eV to clearly show the suppression of the edge modes contribution to the electronic conductance near connection regions. As a result, the peak value of the thermopower for this PRZL around zero energy is enhanced to  $23 k_B/e$  ( $1978 \mu\text{V}/\text{K}$ ). On the other hand, for an asymmetric PRZL, the situation is different. Figure 4(a2) displays the LDOS of electrons for this configuration at  $E = 0$  eV. As seen, in this ring-like geometry a new path between the electrodes is observed and the original first conductance plateau still exists (see Figs. 3(b1) 2(b1)), though its height decreases due to blocking the other path of edge modes propagation. To account for these observations, note that for the asymmetric PRZL (symmetric PRZL), the high-energy modes in the terminal are mixed with the high-energy (low-energy) modes in the middle zigzag PNRs (middle armchair PNRs). Therefore, the transporting modes are more significantly affected by scattering for the symmetric than for asymmetric nanorings [42]. Although the

maximum power factor in Fig. 2(b3) is about the same as the one in Fig. 3(a3), the crucial point here is that by making such nanorings out, we observe a much less electronic thermal conductance  $\kappa_e$  (see Fig. 3(a4)) compared to ZPNRs. Therefore, our designed phosphorene-based nanostructure can remarkably contribute to the improvement of the figure of merit  $ZT$ .

Next, we examine the impact of the nanoring size on the electronic conductance and thermopower of PRZLs. We focus on the symmetric configuration. Fig. 5 depicts the calculated conductance, SC, power factor, and electronic thermal conductance of two PRZLs with different sets of structure parameters. Figs. 5(a1)-(a4) and (b1)-(b4) show the results for the first set of parameters  $W_{in} = 2$  nm,  $L_{in} = 74$  nm,  $W_{out} = 8$  nm,  $L_{out} = 80$  nm, and  $W_L = 4$  nm, and the second set of structure parameters  $W_{in} = L_{in} = W_{out}/2 = L_{out}/2 = W_L = 4$  nm, respectively. The results clearly show that the thermopower profoundly depends on the size of considered nanorings. In general, the smaller ring we consider, the better TE response we get. So, in the second case, the maxima  $S$  enhances and leads to a peak value of  $33 k_B/e$  ( $2830 \mu\text{V/K}$ ) at the zero energy.

In addition, the SC spectrum of the PRZL exhibits some other small oscillations at higher chemical potentials yielding changes in the sign. Figures 6(a1) and (a2) show a zoomed-in view of Figs. 5(b1) and (b2) in the energy range of 1.65 to 1.78 eV. As seen, the transmission coefficient shows Fano line shapes that do not exist in ZPNRs. We have shown in Fig. 6(a3) the LDOS of the Fano resonance peak. The reason behind the appearance of Fano resonance peaks is the interaction between the electronic states of the ring and connected leads. As seen, the mentioned LDOS shows localized states in some regions of the ring implying that the Fano resonances are closely related to the appearance of these bound states [43]. Interestingly, when the chemical potential is tuned near a Fano resonance in the transmission, an enhancement in the thermopower of the nanoring is observed. This is justified as follows. We suppose that the chemical potential locates near a Fano-like antiresonance. According to Eq. (5), the thermopower  $S$  is proportional to  $K_1$  whose value is assessed by the integrand  $(-\frac{\partial f_0}{\partial E})(E - \mu)T_{LR}(E)$  where  $(E - \mu)$  is an odd function around  $\mu$ . As a result, a larger asymmetry of transmission coefficient  $T_{LR}(E)$  leads to an increase in  $K_1$ , and thus a higher TE response.

Now, let us examine the effect of applying a perpendicular magnetic field on the TE performance of a PRZL. It has been shown [5] that by applying a perpendicular magnetic field to PNRs, the conductance experiences dramatic oscillations at special Fermi energies, leading to a giant magnetoresistance (MR) in zigzag PNRs. Here, we show that the TE performance of a PRZL highly depends on the magnetic flux. We only focus on the symmetric case because in this configuration the thermopower changes more rapidly compared to the ZPNRs. Fig. 7(a) depicts the contour plot of the conductance as

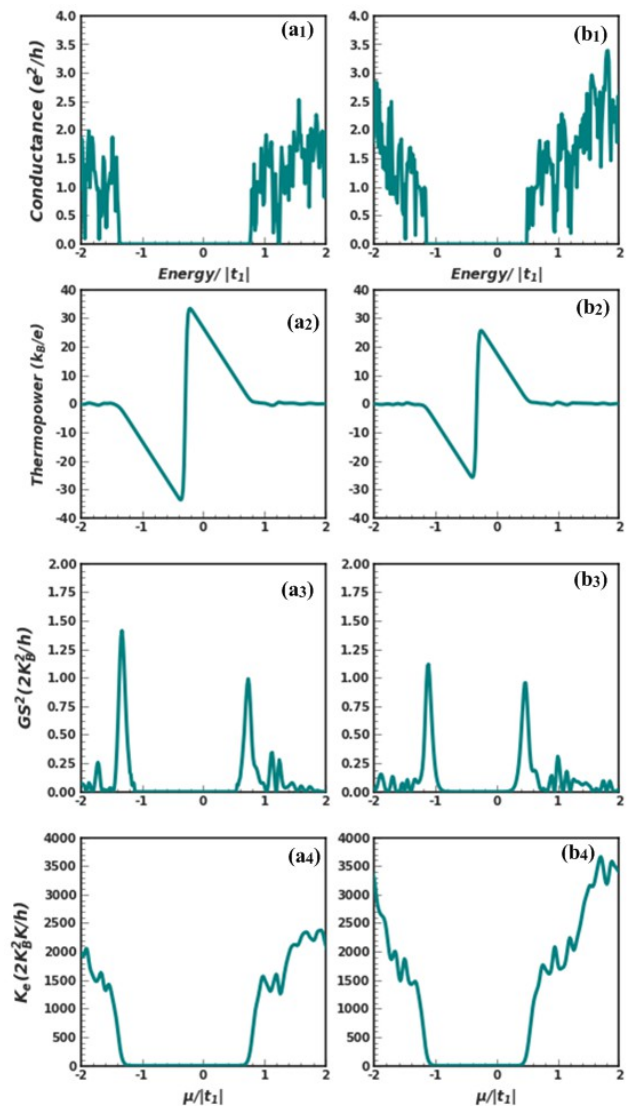


FIG. 5. (a1)-(a4) electronic conductance, thermopower, electronic thermal conductance, and power factor a function of chemical potential for a symmetric PRZL with set of parameters  $k_B T = 0.03|t_1|$ ,  $B = 0$ ,  $W_{in} = 2$  nm,  $L_{in} = 74$  nm,  $W_{out} = 8$  nm,  $L_{out} = 80$  nm,  $W_L = 4$  nm. (b1)-(b4) the same quantities for another symmetric PRZL with the set of parameters  $k_B T = 0.03|t_1|$ ,  $B = 0$ ,  $W_{in} = L_{in} = W_{out}/2 = L_{out}/2 = W_L = 4$  nm.

a function of the applied magnetic field and the Fermi energy for a symmetric PRZL with structure parameters  $W_{in} = 2$  nm,  $L_{in} = 74$  nm,  $W_{out} = 8$  nm,  $L_{out} = 80$  nm, and  $W_L = 4$  nm. Note that here we have increased the size of the nanoring to reduce its oscillation period in the presence of the magnetic field. In this situation, the effective area of the nanoring is relatively large, and as a result, the period of AB oscillations is small which makes it experimentally feasible. We approximate the period of oscillation as  $\Delta B = 2\pi\phi_0/\bar{S}$ , where  $\bar{S} = (S_{in} + S_{out})/2$  is the average area of the outer and inner nanorings. In our case, the average area is  $472.41 \text{ nm}^2$ , yielding the oscill-

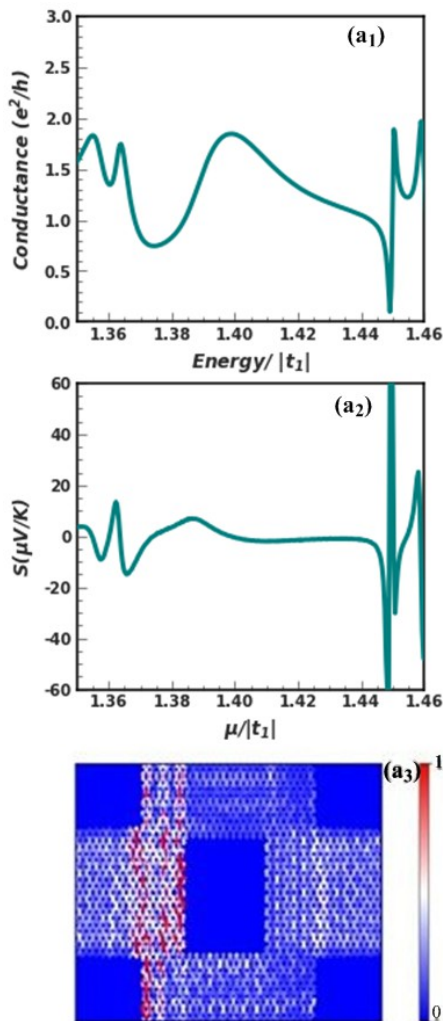


FIG. 6. (a1) and (a2) are zoomed-in views of Figs. 5(b1) and (b2) in the energy range of 1.65 to 1.78 eV, respectively. (a3) LDOS of the Fano resonance peak.

lation period of  $\Delta B \approx 8.73 T$ . As seen in Fig. 7(a), the conductance exhibits an oscillative behavior as a function of the applied magnetic field with a period of  $\sim 8.7 T$  which agrees very well with our theoretical prediction. As seen from Figs. 7(b) and (c), the electronic conductance  $G$  and the thermopower  $S$  also have a periodic character by changing the magnetic field. This leads to a drastic increase in the thermopower  $S$  near an anti-resonance point. Two salient features that we realize from these figures are the high tunability of the thermopower and the possibility to switch on and off the thermoelectric response of the phosphorene nanoring with the magnetic flux. Remarkably, the differential SC can be about eight times larger than the one in the absence of the magnetic field. This confirms the excellent thermoelectric response of this phase-coherent mesoscopic device, making it a promising quantum heat engine in a closed-circuit configuration [44].

Finally, we examine the thermoelectric performance of

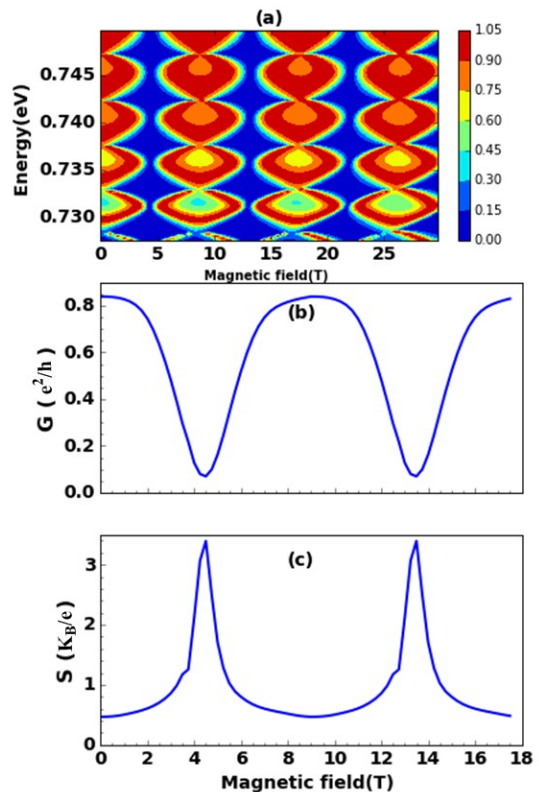


FIG. 7. (a) Contour plot of the electronic conductance as a function of the applied magnetic field and the Fermi energy at temperature  $T = 0$  for a symmetric PRZL. The set of parameters are  $k_B T = 0.03|t_1|$ ,  $W_{in} = 2 \text{ nm}$ ,  $L_{in} = 74 \text{ nm}$ ,  $W_{out} = 8 \text{ nm}$ ,  $L_{out} = 80 \text{ nm}$ , and  $W_L = 4 \text{ nm}$ . (b) The electronic conductance of the symmetric PRZL at  $E_f = 0.732 \text{ eV}$  and  $T = 0$ .

a phosphorene ring with armchair leads (PRAL). Figure 8 depicts the same quantities as in Fig. 3 for both symmetric ((a1)-(a4)) and asymmetric ((b1)-(b4)) connection configurations. A comparison between the two nanostructures shows that for PRALs, the conductance increases in the asymmetric case. The reason for this observation is that for the asymmetric PRAL, the high-energy modes in the terminal are mixed with the high-energy modes of the middle armchair PNRs. This phenomenon occurs oppositely for a quantum dot ring geometry. To further clarify our statement, we have shown in Fig. 9 the spatial LDOS of the transport modes at  $E = 2 \text{ eV}$ . As seen, in the symmetric case (Fig. 9 (a2)), the wave packets of electrons are mainly bounded in the attached left and right leads, and one can find fewer bound states in the central device. This reduces the propagation probability of electrons from the left lead to the right one or vice versa. On the other hand, the LDOS of the asymmetric configuration exhibits more bounding states in the central device, and thus increase the probability of electron transmission which emerges as conductance peaks. The SCs for both the symmetric and asymmetric PRALs are about the same as that of AP-

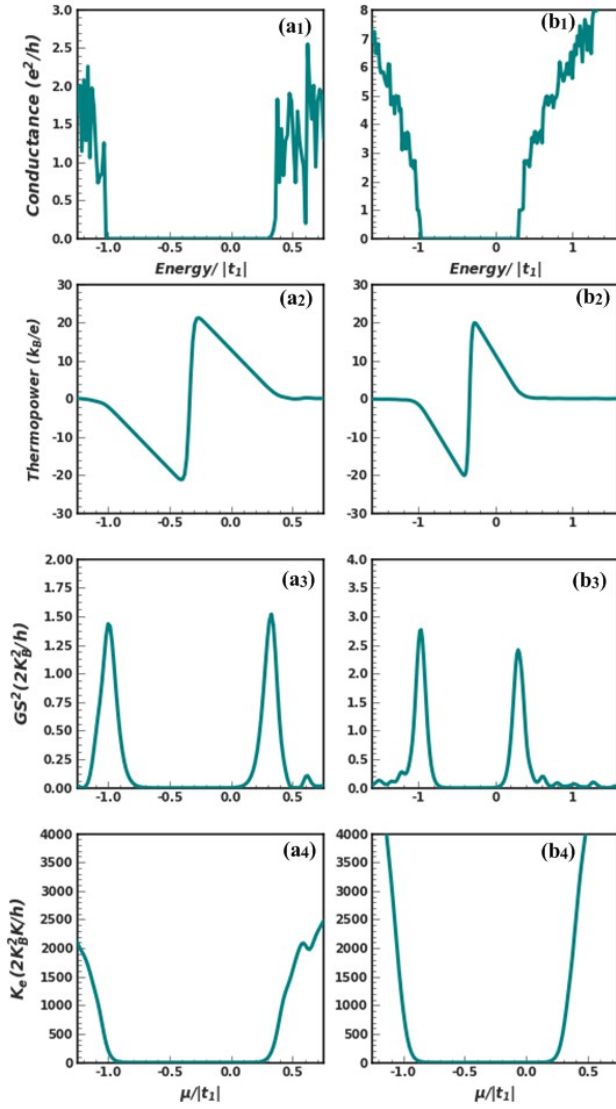


FIG. 8. The same quantities as in Fig. 3 for both (a1)-(a4) symmetric and (b1)-(b4) asymmetric coupling of two armchair leads to the ring.

NRs. Here, the reason is that we have no suppressed edge modes in the ribbons, and thus the band gap remains almost intact. Intriguingly, for PRALs the electronic thermal conductance (see Figs. 8(a4) and (b4)) can be about ten times smaller than that of APNRs (see Fig. 2(a4)). As a result, one expects to observe a remarkable improvement in the figure of merit  $ZT$  for these phosphorene-based nanostructures. The behavior of PRALs by changing the size of the ring and by applying the perpendicular magnetic field is similar to PRZLs and we do not present the results here.

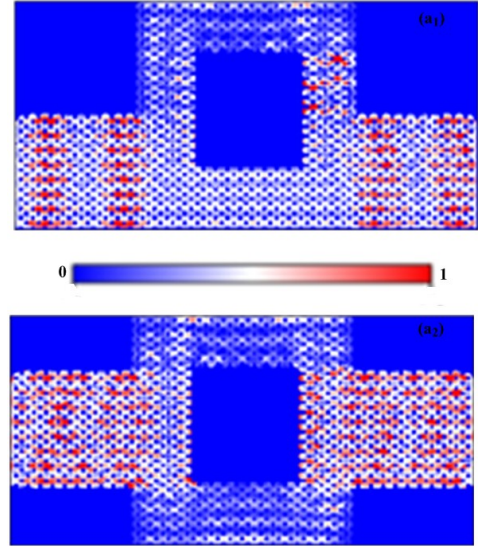


FIG. 9. Spatial LDOS for (a) a symmetric and (b) an asymmetric PRAL at  $E_f = 2$  eV.

#### IV. SUMMARY AND CONCLUSION

In summary, we investigated the thermoelectric properties of different phosphorene nanorings with symmetrical or asymmetrical connection configurations. We utilized the effective low-energy TB model of monolayer phosphorene to construct the TB Hamiltonian of our designed devices and to characterize their electronic conductance, thermopower, and thermal conductance within the Landauer-Buttiker formalism. We first examined the TE performance of phosphorene nanoribbons to validate our model by comparison with other works and then studied the conductance and TE properties of our systems. Our results showed that the quantum interference of localized electronic states in the nanorings and the electronic wave packets of leads profoundly affect the TE properties of the system. We found that for a symmetrical connection of zigzag leads to rectangular rings, the original first conductance plateau completely collapses due to the suppression of the contribution of edge states. This induces a wide gap in the system, giving rise to dramatically enhanced peak values in thermopower of such configurations. We also have shown that the TE performance of these systems depends on the size of the ring and one can reach the maximum amount of  $33k_B/e$  ( $2830 \mu\text{V/K}$ ) for the thermopower. The appeared Fano antiresonances in the quantum conductance of phosphorene nanorings lead to characteristic features in the Seebeck coefficient. We showed the tunability of the thermopower and the possibility to switch on and off the thermoelectric response of phosphorene nanorings by controlling the applied magnetic field. For nanorings with attached armchair phosphorene nanoribbons, our calculations revealed that though the thermopower almost remains intact, a remarkable decrease in the electronic conductivity oc-

curs. This can lead to a notable improvement in the figure of merit of these systems. Our study confirmed

the promising thermoelectric properties of these phase-coherent mesoscopic devices and propose them as potential thermoelectric candidates.

- 
- [1] I. Petsagkourakis, K. Tybrandt, X. Crispin, I. Ohkubo, N. Satoh, and T. Mori, *Science and technology of advanced materials* **19**, 836 (2018).
- [2] J. R. Szczech, J. M. Higgins, and S. Jin, *Journal of Materials Chemistry* **21**, 4037 (2011).
- [3] C. Hozana and A. Latgé, *Journal of Physics: Condensed Matter* **31**, 125303 (2019).
- [4] F. Mazzamuto, V. H. Nguyen, Y. Apertet, C. Caër, C. Chassat, J. Saint-Martin, and P. Dollfus, *Physical Review B* **83**, 235426 (2011).
- [5] R. Zhang, Z. Wu, X. J. Li, and K. Chang, *Physical Review B* **95**, 125418 (2017).
- [6] Y. Liu and X. Yang, *Journal of Applied Physics* **108**, 023710 (2010).
- [7] G. Haack and F. Giazotto, *Physical Review B* **100**, 235442 (2019).
- [8] E. Samuel Reich, *Nature News* **506**, 19 (2014).
- [9] L. Li, F. Yang, G. J. Ye, Z. Zhang, Z. Zhu, W. Lou, X. Zhou, L. Li, K. Watanabe, T. Taniguchi, *et al.*, *Nature nanotechnology* **11**, 593 (2016).
- [10] L. Li, Y. Yu, G. J. Ye, Q. Ge, X. Ou, H. Wu, D. Feng, X. H. Chen, and Y. Zhang, *Nature nanotechnology* **9**, 372 (2014).
- [11] H. Liu, A. T. Neal, Z. Zhu, Z. Luo, X. Xu, D. Tománek, and P. D. Ye, *ACS nano* **8**, 4033 (2014).
- [12] F. Xia, H. Wang, and Y. Jia, *Nature communications* **5**, 1 (2014).
- [13] A. Castellanos-Gomez, L. Vicarelli, E. Prada, J. O. Island, K. Narasimha-Acharya, S. I. Blanter, D. J. Groenendijk, M. Buscema, G. A. Steele, J. Alvarez, *et al.*, *2D Materials* **1**, 025001 (2014).
- [14] S. P. Koenig, R. A. Doganov, H. Schmidt, A. Castro Neto, and B. Özyilmaz, *Applied Physics Letters* **104**, 103106 (2014).
- [15] J. Qiao, X. Kong, Z.-X. Hu, F. Yang, and W. Ji, *Nature communications* **5**, 1 (2014).
- [16] M. Buscema, D. J. Groenendijk, S. I. Blanter, G. A. Steele, H. S. Van Der Zant, and A. Castellanos-Gomez, *Nano letters* **14**, 3347 (2014).
- [17] S. Das, W. Zhang, M. Demarteau, A. Hoffmann, M. Dubey, and A. Roelofs, *Nano letters* **14**, 5733 (2014).
- [18] W. Lu, H. Nan, J. Hong, Y. Chen, C. Zhu, Z. Liang, X. Ma, Z. Ni, C. Jin, and Z. Zhang, “Nano res. 7, 853 (2014),”.
- [19] A. Rodin, A. Carvalho, and A. C. Neto, *Physical review letters* **112**, 176801 (2014).
- [20] X. Chen, Y. Wu, Z. Wu, Y. Han, S. Xu, L. Wang, W. Ye, T. Han, Y. He, Y.-a. Cai, *et al.*, *Nature communications* **6**, 1 (2015).
- [21] V. Tayari, N. Hemsworth, I. Fakhri, A. Favron, E. Gaufres, G. Gervais, R. Martel, and T. Szkopek, *Nature communications* **6**, 1 (2015).
- [22] Y.-L. Zou, J. Song, C. Bai, and K. Chang, *Physical Review B* **94**, 035431 (2016).
- [23] Q. Wei and X. Peng, *Applied Physics Letters* **104**, 251915 (2014).
- [24] J. Island, G. Steele, H. Van Der Zant, and A. Castellanos-Gomez, “2d mater. 2, 011002 (2015),”.
- [25] M. Ezawa, *New Journal of Physics* **16**, 115004 (2014).
- [26] A. Castellanos-Gomez, *The journal of physical chemistry letters* **6**, 4280 (2015).
- [27] E. Flores, J. R. Ares, A. Castellanos-Gomez, M. Barawi, I. J. Ferrer, and C. Sánchez, *Applied Physics Letters* **106**, 022102 (2015).
- [28] Y. Saito, T. Iizuka, T. Koretsune, R. Arita, S. Shimizu, and Y. Iwasa, *Nano letters* **16**, 4819 (2016).
- [29] A. Carvalho, M. Wang, X. Zhu, A. S. Rodin, H. Su, and A. H. Castro Neto, *Nature Reviews Materials* **1**, 1 (2016).
- [30] R. Fei, A. Faghaninia, R. Soklaski, J.-A. Yan, C. Lo, and L. Yang, *Nano letters* **14**, 6393 (2014).
- [31] J. Zhang, H. Liu, L. Cheng, J. Wei, J. Liang, D. Fan, J. Shi, X. Tang, and Q. Zhang, *Scientific reports* **4**, 1 (2014).
- [32] R. Ma, H. Geng, W. Deng, M. Chen, L. Sheng, and D. Xing, *Physical Review B* **94**, 125410 (2016).
- [33] S. Lee, J.-P. Song, S.-H. Kang, and Y.-K. Kwon, *Scientific reports* **11**, 1 (2021).
- [34] M. C. Watts, L. Picco, F. S. Russell-Pavier, P. L. Cullen, T. S. Miller, S. P. Bartuš, O. D. Payton, N. T. Skipper, V. Tileli, and C. A. Howard, *Nature* **568**, 216 (2019).
- [35] M. Saiz-Bretín, A. Malyshev, P. Orellana, and F. Domínguez-Adame, *Physical Review B* **91**, 085431 (2015).
- [36] A. N. Rudenko and M. I. Katsnelson, *Physical Review B* **89**, 201408 (2014).
- [37] C. W. Groth, M. Wimmer, A. R. Akhmerov, and X. Waintal, *New Journal of Physics* **16**, 063065 (2014).
- [38] Y. Imry and R. Landauer, *Reviews of Modern Physics* **71**, S306 (1999).
- [39] S. Datta, *Electronic transport in mesoscopic systems* (Cambridge university press, 1997).
- [40] S.-H. Lv and Y.-X. Li, *Journal of Applied Physics* **112**, 053701 (2012).
- [41] D. Moldovan and F. Peeters, *Zenodo* **826942** (2017).
- [42] Z. Wu, Z. Zhang, K. Chang, and F. Peeters, *Nanotechnology* **21**, 185201 (2010).
- [43] R. Zhang, Z. Wu, X. Li, L. Li, Q. Chen, Y.-M. Li, and F. Peeters, *Nanotechnology* **29**, 215202 (2018).
- [44] H. Li, Y. Wang, X. Kang, S. Liu, and R. Li, *Journal of Applied Physics* **121**, 065105 (2017).
- [45] S. Lee, F. Yang, J. Suh, S. Yang, Y. Lee, G. Li, H. S. Choe, A. Suslu, Y. Chen, C. Ko, *et al.*, *Nature communications* **6**, 1 (2015).
- [46] J. Pang, A. Bachmatiuk, Y. Yin, B. Trzebicka, L. Zhao, L. Fu, R. G. Mendes, T. Gemming, Z. Liu, and M. H. Rummeli, *Advanced Energy Materials* **8**, 1702093 (2018).
- [47] E. T. Sisakht, M. H. Zare, and F. Fazileh, *Physical Review B* **91**, 085409 (2015).
- [48] S. Mahnia and A. Phirouznia, *Journal of Computational Electronics* **13**, 224 (2014).
- [49] Z. Zhang, K. Chang, and K. S. Chan, *Applied Physics Letters* **93**, 062106 (2008).



- [50] V. M. García-Suárez, R. Ferradás, and J. Ferrer, Physical review b **88**, 235417 (2013).